JP Journal of Heat and Mass Transfer

https://pphmjopenaccess.com
https://doi.org/10.17654/0973576324024
Volume 37, Number 3, 2024, Pages 349-364 **P-ISSN: 0973-5763**

ENHANCING ENERGETIC EFFICIENCY: ADVANCING MORPHOLOGICAL AND THERMAL STRUCTURAL PROPERTIES OF FLY ASH AND CERAMIC-BASED MATERIALS

Hajar Sdira[1], Laila Farissi[2], Mohammed Ali Arbaoui[3], Mohamed Waqif[2], Asmae Arbaoui[1], Latifa Saadi[2], Mouhaydine Tlemçani[4] and Amal Bouich[5]

[1]Thermodynamic Energy Laboratory (LTE)
Faculty of Sciences
Mohammed V University
1014 Rabat, Morocco

[2]Laboratory of Innovative Materials,
Energy and Sustainable Development (IMED-Lab)
Faculty of Science and Technology of Marrakesh
Cadi Ayyad University
549, Marrakech, Morocco

Received: March 5, 2024; Accepted: April 18, 2024

Keywords and phrases: clay, fly ash, XRD, SEM, EDS, FTIR, structural and thermal properties.

How to cite this article: Hajar Sdira, Laila Farissi, Mohammed Ali Arbaoui, Mohamed Waqif, Asmae Arbaoui, Latifa Saadi, Mouhaydine Tlemçani and Amal Bouich, Enhancing energetic efficiency: advancing morphological and thermal structural properties of fly ash and ceramic-based materials, JP Journal of Heat and Mass Transfer 37(3) (2024), 349-364. https://doi.org/10.17654/0973576324024

Published Online: June 3, 2024

[3]Design and Systems Laboratory (Electronics, Signals and IT) (LCS)
Faculty of Sciences
Mohammed V University
1014 Rabat, Morocco

[4]Department of Informatics
School of Sciences and Technology
University of Évora
7004-516 Évora, Portugal

[5]Institut de Disseny per a la Fabricació Producció Automatitzada
Universitat Politècnica de València
46022 Valencia, Spain

Abstract

Herein, we investigate structural and thermal characteristics of clay, fly ash, and their respective mixtures, with a particular focus on the influence of sintering. Employing a comprehensive suite of analytical techniques, including X-ray fluorescence analysis (XRF), scanning electron microscopy (SEM), X-ray diffraction (XRD), and Fourier transform infrared spectroscopy, the inquiry seeks to elucidate the intricate alterations and transformations arising from the sintering process and the integration of fly ash.

The calcination process applied to the raw materials resulted in the formation of diverse phases, including enstatite, spinel, anorthite, mullite, corundum, and cristobalite. Similarly, the fly ash/clay mixtures exhibited distinct phases, such as wollastonite, periclase, and cordierite, indicative of the structural changes induced by the sintering process. The application of SEM further provided insights into the morphological characteristics of the raw materials, revealing variations in shapes and sizes, thereby contributing to a comprehensive understanding of the compositional and structural modifications incurred during sintering. These phases guarantee thermal stability, ensuring the production of lightweight ceramics materials characterized by low thermal conductivities and high strength. These materials present themselves as promising candidates for applications in refractory settings.

1. Introduction

The escalating demand for materials exhibiting diverse properties, encompassing chemical, mechanical, thermal, and environmental attributes, has underscored the imperative for continuous research and development in the realm of ceramic materials. This pursuit is pivotal in advancing technological and industrial domains while preserving environmental integrity. Within this context, the investigation into refractory ceramics has gained prominence, particularly those rich in alumina due to their consequential mechanical, thermal, and electrical properties [1]. However, the conventional sintering processes employed for these materials necessitate exceedingly high temperatures, contributing to substantial energy consumption and environmental degradation [2].

To address these challenges, the current study endeavors to formulate novel mixtures by combining ceramic materials with low thermal resistance components, with the objective of achieving consolidation at lower temperatures. The significance and value of this research lie in its potential to mitigate the environmental impact associated with traditional sintering techniques.

Central to this investigation is the exploration of fly ash, a predominant byproduct of coal combustion in power plants. The composition of fly ash, characterized by its significant aluminum and silicon content, closely mirrors that of various ceramic materials, making it a subject of considerable interest in numerous studies, particularly those examining its application in the production of cordierite [3] and mullite [4] ceramics. Despite its potential, coal fly ash contributes significantly to environmental concerns, precipitating water, air, and soil contamination [5]. Notably, the global production of coal fly ash is estimated at a staggering 780 million metric tons [6]. Although utilized to some extent in construction materials, not exceeding 25 wt.% of its total production [7], the imperative to discover novel approaches for recycling fly ash remains of paramount importance.

Moreover, a concurrent exploration into the amalgamation of fly ash with steel slag is presented, with a focus on the effect of the CaO/SiO_2 ratio on phase transitions. This study resulted in the development of optimized anorthite-based ceramics, exhibiting notable thermal and dielectric properties, presenting potential applications in insulation technology [8]. Furthermore, investigations into the combination of fly ash and steel slag illuminated the effects of cordierite crystallization with the anorthite phase, yielding ceramics with promising mechanical strength, thermal properties, and applicability in electronic devices [9].

Consequently, the principal objective of this study is to evaluate a local clay by incorporating varying proportions of fly ash sourced from thermal power stations. This evaluation aims to discern the influence of fly ash addition on the thermal and chemical properties of clay, contributing to a nuanced understanding of sustainable material utilization in diverse applications.

2. Materials and Methods

2.1. Samples sources

The specimens under investigation were derived from distinct source materials, namely red clayey soil (Arg.b) procured from the Demnate site in close proximity to Marrakech, and industrial waste in the form of fly ash (C.V) generated at the Jorf Lasfar office situated in the city of El Jadida.

2.2. Preparation of test samples

A beaker containing 10g of the composite mixture was subjected to the addition of 150ml of distilled water. Following a 30-minute stirring period, the resulting mixtures were subsequently transferred to an oven set at 100°C for a duration of 24 hours. The resulting powder underwent a grinding process and subsequent heat treatment within a muffle furnace, where varying temperatures (900°C, 1000°C, 1100°C, and 1150°C) were applied

for two hours at a controlled heating rate of 1°C/min. The comprehensive mass percent composition of the formulated mixtures is presented in Table 1.

Table 1. Mass percent composition of the prepared formulations

Formulations/component	Mass percent of mixtures component %	
	Arg.b	C.V
$ArgCV_5$	50	50
$ArgCV_9$	10	90
$ArgCV_7$	30	70
Clay (Arg.b)	100	-
Fly ash (C.V)	-	100

2.3. Characterization techniques

Various experimental techniques were applied to the raw, calcined, and sintered powder samples. The chemical composition of the initial materials was determined through X-ray fluorescence analysis (XRF) utilizing the "Philips PW X'PERT MPD" X-ray diffractometry device, employing a wavelength of K = 1.5406Å and scanning within the interval [5°, 80°]. X-ray diffraction analysis (XRD) was performed on both raw and calcined materials using the same device, scanning within the range [5°, 80°] and employing a wavelength of K = 1.5406Å.

Fourier transform infrared spectroscopy (FTIR) analysis was conducted on raw and calcined materials using pellets containing 1% of the mass of the mixture and 99% potassium bromide (KBr). This analysis was carried out with a Fourier transform spectrometer (VERTEX 70) over a wave number range of 400cm^{-1} to 4000cm^{-1}.

Morphological analysis of the raw powder was executed using a scanning electron microscope (SEM) equipped with an EDS detector (Falcon EDAX) on a TESCAN VEGA3.

3. Results and Discussion

3.1. Chemical composition (XRF) of starting materials

The X-ray fluorescence (XRF) analysis of raw materials, as depicted in (Table 2) reveals notable compositions in the clay sample, particularly substantial percentages of silica (30.99% SiO_2) and alumina (10.49% Al_2O_3). Additionally, the clay sample exhibits elevated levels of MgO and CaO compared to other oxide contents. In contrast, the fly ash analysis indicates a predominant presence of silica (48.84%) and alumina (32.79%), accompanied by significant percentages of Fe_2O_3, CaO, and MgO. Traces of K_2O, P_2O_5, Na_2O, and SO_3 are also observed.

This analysis underscores that fly ash primarily comprises silica and alumina, which contribute to the refractory characteristics of ceramic materials. However, it also contains noteworthy quantities of oxides with a melting nature, including Fe_2O_3, CaO, K_2O, Na_2O, and MgO.

Table 2. XRF analysis of raw materials

Samples	Arg.b	C.V
SiO_2 %	30,99	48,84
Al_2O_3 %	10,49	32,79
MgO %	6,18	1,46
Fe_2O_3 %	0,67	6,12
K_2O %	2,4	1,12
TiO_2 %	0,47	-
CaO %	4,1	4,37
P_2O_5 %	-	0,51
Na_2O %	-	0,06
SO_3 %	-	0,44

3.2. Mineralogical composition (X-rays and FTIR) of starting materials

The X-ray diffractograms (Figure 1) and FTIR spectra (Figure 2) of the initial samples (Arg.b and C.V) demonstrate distinct mineralogical compositions between the two specimens. The X-ray diffraction spectrum of

Demnate clay (Arg.b) exhibits characteristic peaks associated with quartz (Q), vermiculite (V), kaolinite (K), muscovite (M), and hematite (H). Conversely, the X-ray diffraction spectrum of fly ash (C.V) indicates the presence of characteristic peaks for quartz (Q) and mullite (M). The affirmation of these identified phases is further supported by the infrared analysis.

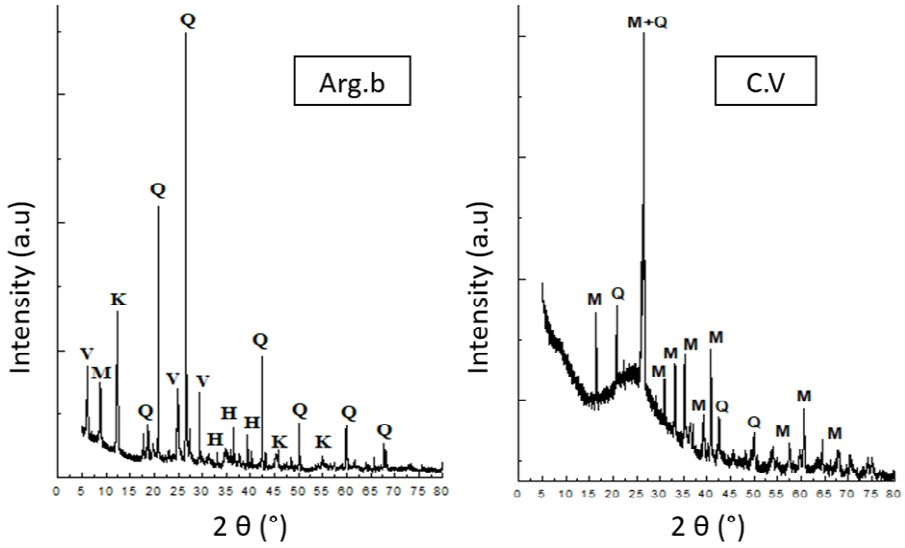

Figure 1. XRD spectrum of untreated raw materials.

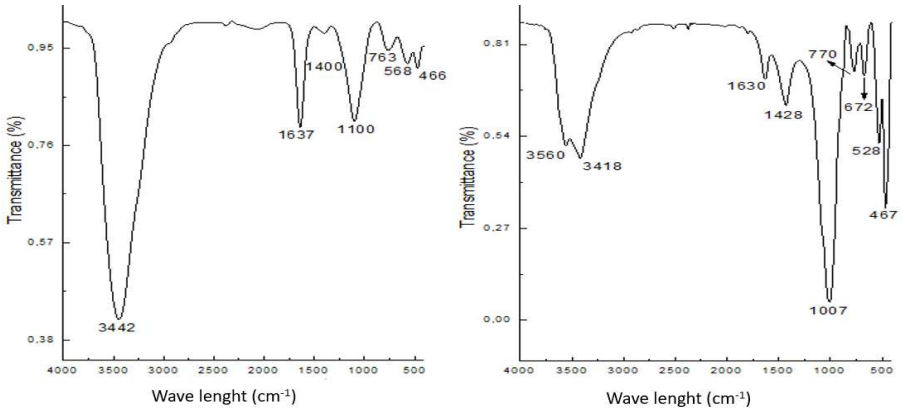

Figure 2. FTIR pattern of untreated raw materials.

Notably, the X-ray diffractograms within the 20 to 30 range in (Figure 1), depicting the raw materials, reveal a curve not aligned with the baseline. This deviation is attributed to the presence of an amorphous phase high in silica, a characteristic that is duly corroborated by the observation of an infrared absorption band at 1000°C (Figure 2) [10]. The corresponding IR spectrum table is presented in Table 3.

Table 3. FTIR spectrum assignments

Bands cm^{-1}	Assignement	References
3560-3418	O-H bond valence vibrations	[11]
3442	Vibrations elongations of the O-H bond	[12]
1630-1637	O-H bond deformation vibrations of absorbed water	[13, 14]
1428-1400	C-O bond valence vibrations of carbonate phase	[15]
1007	Valence vibrations of the Si-O bond (kaolinite)	[16]
770	Quartz	[17]
672	OH deformation vibrations	
467	Vibrations elongations of the Si-O-Si bond	[18]
568-528-1100	Vibrations of the Si-O-Al bond	[19]
763	Vibrations elongations of the Al-O bond	[8]

3.3. Morphology of raw materials

The results derived from the Scanning Electron Microscope (SEM) analysis (Figure 3) and the chemical composition determined through Energy Dispersive X-ray spectroscopy (EDX) (Figures 4 and 5) conducted on the initial materials, namely fly ash and clay, reveal distinct morphologies characterized by various shapes and sizes.

The SEM images illustrate that clay particles manifest as clusters of fine aggregates and thin pseudo hexagonal platelets, indicative of kaolinite (K). Additionally, quartz crystals are identified within the clay composition. In contrast, fly ash particles appear as isolated and contiguous spheres, some exhibiting hollows, along with cenospheres of varying sizes. The smallest of these, microspheres, are discernible within pherospheres. The EDX/SEM analysis underscores that Al, Si and O constitute the principal elements of

fly ash, with a division into two components: a crystalline phase (mineral) encompassing quartz and spherical mullite, and an amorphous glass phase (silica) [20].

Furthermore, the EDX analysis of the Arg.b and C.V samples serves to validate the chemical compositions ascertained through X-ray fluorescence analysis.

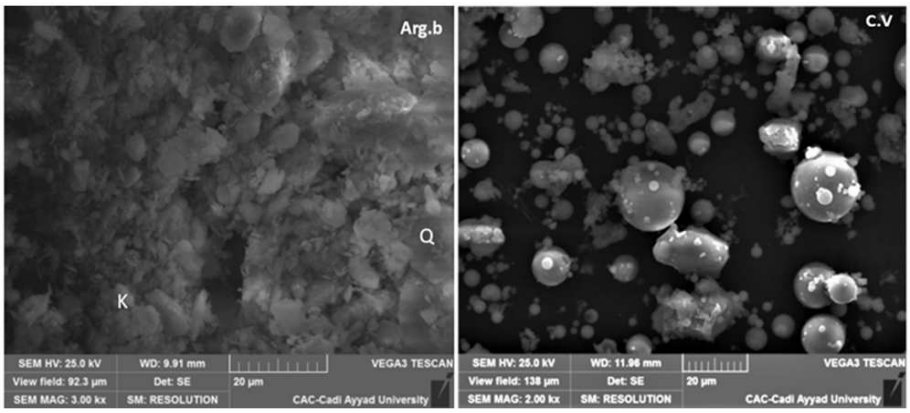

Figure 3. SEM image of untreated raw materials.

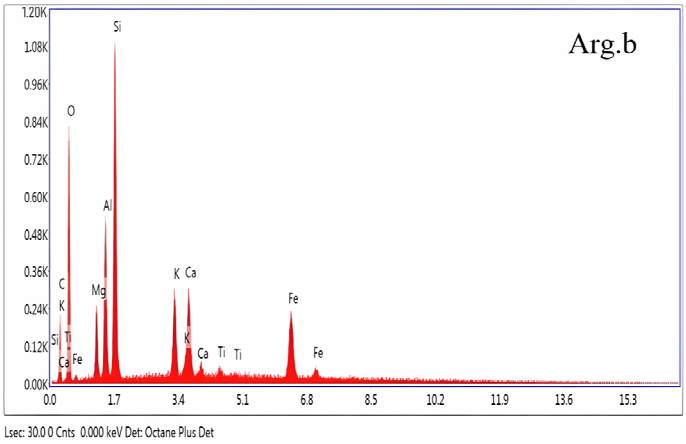

Figure 4. EDX analysis of untreated clay (Arg.b).

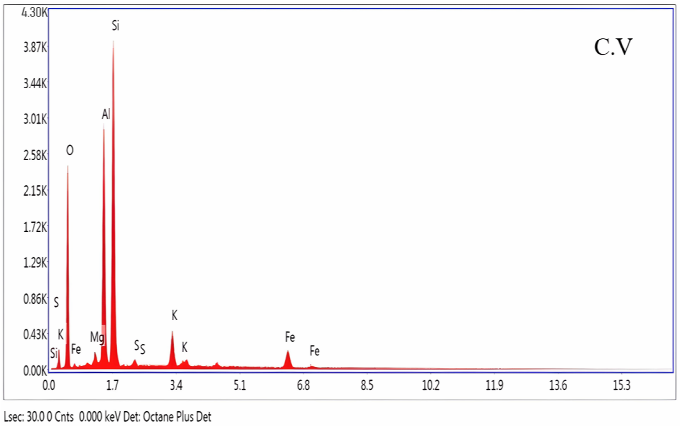

Figure 5. EDX analysis of untreated fly ash (C.V).

3.4. Effect of calcination temperature on phase evolution

The X-ray diffractograms and FTIR spectra of the initial samples calcinated at 1100°C and 1150°C are presented in Figures 6 and 7, respectively. The results reveal that the mineralogical composition of each sample undergoes variations contingent upon the calcination temperature.

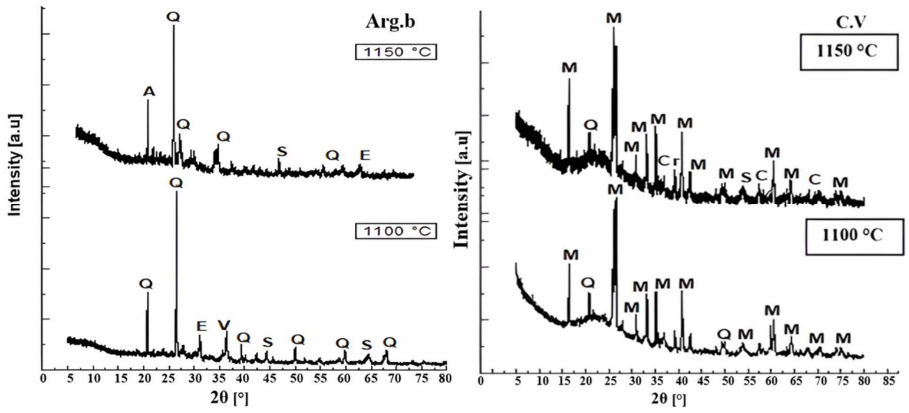

Figure 6. XRD pattern of treated raw materials at 1000°C and 1150°C (Arg.b and C.V).

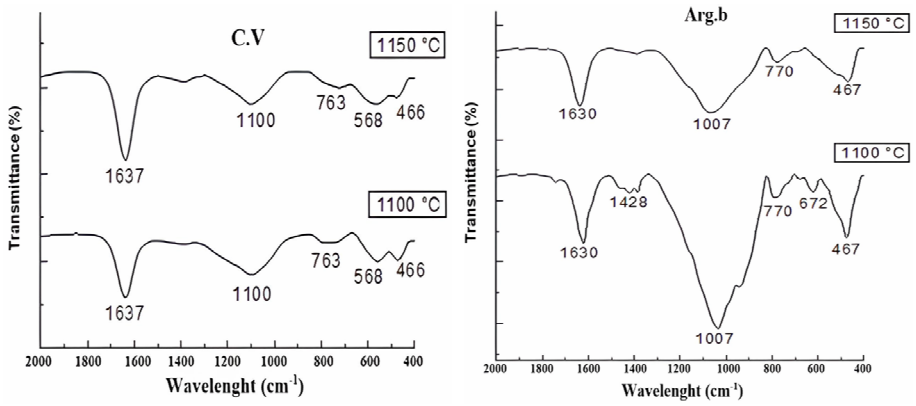

Figure 7. FTIR spectrum of treated raw materials at 1000°C and 1150°C (Arg.b and C.V).

In the X-ray diffraction spectrum of Demnate clay (Arg.b), characteristic peaks of quartz (Q), vermiculite (V), enstatite (E), spinel (S), and anorthite (A) are discerned. Also, the disappearance of kaolinite (K), muscovite (M), and hematite (H) is noted in both samples, with vermiculite (V) vanishing at 1150°C. Specifically, the X-ray diffraction of Arg.b calcinated at 1150°C exhibits characteristic lines of quartz (Q), anorthite (A), enstatite (E), and spinel (S), while at 1100°C, it shows those of quartz (Q), enstatite (E), vermiculite (V), and spinel (S). The presence of these phases is corroborated by infrared analysis, where the absence of the Si-O-Al band at 1100°C is observed, along with the absence of bands corresponding to the deformation of OH and valence vibrations of the CO bond due to the temperature increase up to 1150°C.

The X-ray diffraction spectrum of fly ash (C.V) calcinated at 1100°C reveals the presence of characteristic peaks of mullite (M) and quartz (Q). At 1150°C, in addition to the previously mentioned phases, a crystallization of spinel, corundum, and cristobalite is detected. This crystallization phenomenon is substantiated by the corresponding infrared spectrum.

3.5. Mineralogical composition of ($ArgCV_{i=5,7,9}$) calcinated formulations (X-rays and FTIR)

The X-ray diffractograms (Figure 8) and the FTIR spectra (Figure 9) of the three formulations ($ArgCV_{i=5,7,9}$) subjected to calcination at 1100°C and 1150°C reveal distinct variations in the mineralogical composition of each formulation contingent upon the calcination temperature.

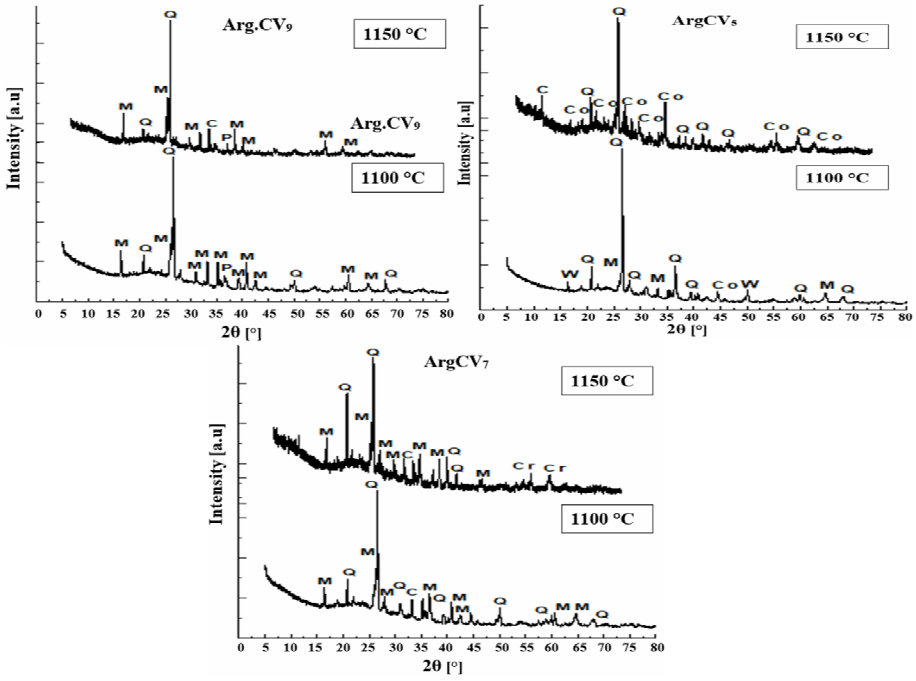

Figure 8. XRD pattern of $ArgCV_{i=5,7,9}$ treated formulations.

In the X-ray diffraction spectrum of $ArgCV_9$, characteristic peaks of quartz (Q), mullite (M), corundum (C), and periclase (P) are evident. Notably, periclase (P) emerges at 1100°C, while corundum (C) and periclase (P) appear at 1150°C. The X-ray diffraction spectrum of $ArgCV_7$ exhibits characteristic peaks of quartz (Q), mullite (M), corundum (C), and cristobalite (Cr). Additionally, corundum (C) emerges at 1100°C, followed by the appearance of both corundum (C) and cristobalite (Cr) at 1150°C. The X-ray diffraction spectrum of $ArgCV_5$ displays characteristic peaks of quartz

(Q), mullite (M), corundum (C), cordierite (Co), and wollastonite (W). Indeed, cordierite (Co) manifests at 1100°C, with both cordierite (Co) and cristobalite (Cr) appearing at 1150°C. The presence of these phases is robustly substantiated and confirmed through infrared analysis.

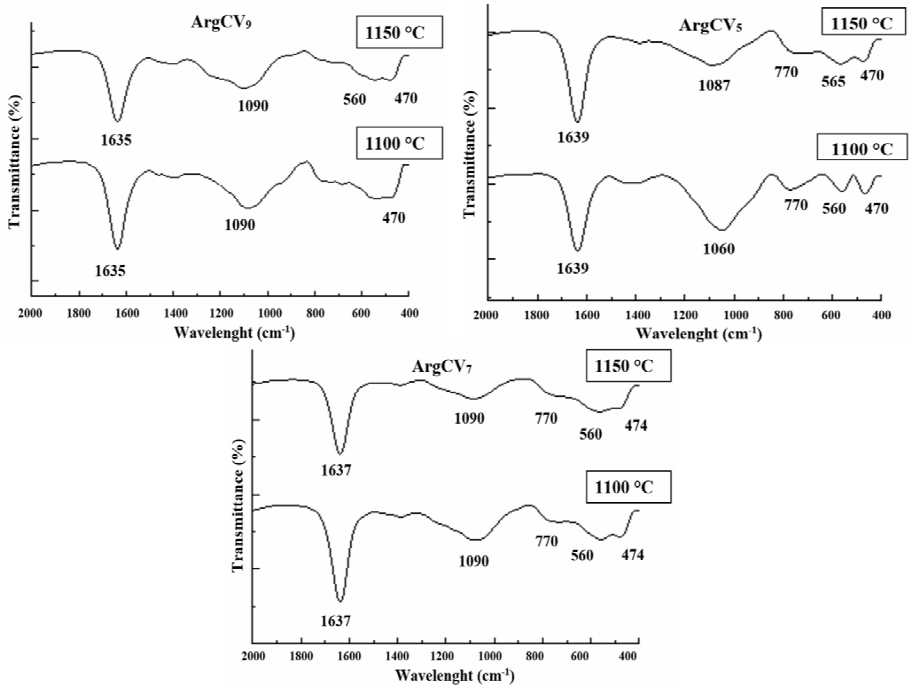

Figure 9. FTIR spectrum of $\mathrm{ArgCV}_{i=5,7,9}$ treated formulations.

4. Conclusion

In conclusion, this study contributes to the advancement of refractory material formulations, aiming to enhance their mechanical properties. The experimental investigation centered on the sintering, physicochemical, and thermal characterization of raw materials (Arg.b and C.V). The chemical analysis of Arg.b revealed a composition encompassing silica, alumina, magnesium oxide, ferric oxide, potassium oxide, titanium dioxide, and calcium oxide, aligning with its mineralogical constituents of quartz, vermiculite, kaolinite, muscovite, and hematite. The mineralogical

composition of Arg.b evolved with the calcination temperature, notably transitioning at 1150°C to include quartz, enstatite, spinel, and anorthite.

Similarly, the chemical analysis of fly ash (C.V) demonstrated a composition comprising silica, alumina, magnesium oxide, ferric oxide, potassium oxide, calcium oxide, phosphorus pentoxide, sodium oxide, and sulfur trioxide, corresponding to its mineralogical constituents of mullite and quartz. The mineralogical composition of C.V also transformed with the calcination temperature, revealing spinel, corundum, and cristobalite at 1150°C. The XRD patterns indicated the emergence of the periclase phase with an increase in C.V percentage and the emergence of cordierite and wollastonite with an increase in Arg.b percentage.

In summary, this research illuminates the intricate interplay among composition, sintering conditions, and structural properties crucial for the advancement of refractory materials. The findings offer valuable insights for optimizing formulations tailored to thermal insulation applications. The identified phases play a pivotal role in ensuring thermal stability, facilitating the production of lightweight ceramic materials with low thermal conductivities and high strength. These materials stand out as promising candidates for a variety of applications within refractory settings.

References

[1] Andrew Ruys, Processing, structure, and properties of alumina ceramics, Alumina Ceramics (2019), 71-121. https://doi.org/10.1016/B978-0-08-102442-3.00004-X.

[2] Andrew Ruys, Processing, structure, and properties of alumina ceramics, Alumina Ceramics (2019), 75-101. https://doi.org/10.1016/B978-0-08-102442-3.00004-X.

[3] Shaoxin Wang, Hao Wang, Ziwei Chen, Ru Ji, Lili Liu and Xidong Wang, Fabrication and characterization of porous cordierite ceramics prepared from fly ash and natural minerals, Ceramics International 45(15) (2019), 18306-18314. https://doi.org/10.1016/j.ceramint.2019.06.043.

[4] Beiyue Ma, Chang Su, Xinming Ren, Zhi Gao, Fan Qian, Wengang Yang, Guoqi Liu, Hongxia Li, Jingkun Yu and Qiang Zhu, Preparation and properties of porous mullite ceramics with high-closed porosity and high strength from fly ash via reaction synthesis process, Journal of Alloys and Compounds 803 (2019), 981-991. https://doi.org/10.1016/j.jallcom.2019.06.272.

[5] N. Güleç, B. (Çanci) Günal and A. Erler, Assessment of soil and water contamination around an ash-disposal site: a case study from the Seyitömer coal-fired power plant in western Turkey, Environmental Geology 40(3) (2001), 331-344. https://doi.org/10.1007/s002540000228.

[6] Z. T. Yao, X. S. Ji, P. K. Sarker, J. H. Tang, L. Q. Ge, M. S. Xia and Y. Q. Xi, A comprehensive review on the applications of coal fly ash, Earth-Science Reviews 141 (2015), 105-121. https://doi.org/10.1016/j.earscirev.2014.11.016.

[7] Arpita Bhatt, Sharon Priyadarshini, Aiswarya Acharath Mohanakrishnan, Arash Abri, Melanie Sattler and Sorakrich Techapaphawit, Physical, chemical, and geotechnical properties of coal fly ash: a global review, Case Studies in Construction Materials 11 (2019), e00263. https://doi.org/10.1016/j.cscm.2019.e00263.

[8] Kamal Tabit, Hanaa Hajjou, Mohamed Waqif and Latifa Saâdi, Effect of CaO/SiO_2 ratio on phase transformation and properties of anorthite-based ceramics from coal fly ash and steel slag, Ceramics International 46(6) (2020), 7550-7558. https://doi.org/10.1016/j.ceramint.2019.11.254.

[9] Kamal Tabit, Mohamed Waqif and Latifa Saâdi, Anorthite-cordierite based binary ceramics from coal fly ash and steel slag for thermal and dielectric applications, Materials Chemistry and Physics 254 (2020), 123472. https://doi.org/10.1016/j.matchemphys.2020.123472.

[10] Milan Kanti Naskar and Minati Chatterjee, A novel process for the synthesis of cordierite ($Mg_2Al_4Si_5O_{18}$) powders from rice husk ash and other sources of silica and their comparative study, Journal of the European Ceramic Society 24(13) (2004), 3499-3508. https://doi.org/10.1016/j.jeurceramsoc.2003.11.029.

[11] Ning Chen, Guodong Fang, Guangxia Liu, Dongmei Zhou, Juan Gao and Cheng Gu, The effects of Fe-bearing smectite clays on OH formation and diethyl phthalate degradation with polyphenols and H_2O_2, Journal of Hazardous Materials 357 (2018), 483-490. https://doi.org/10.1016/j.jhazmat.2018.06.030.

[12] Ling Ding, Xiaoqin Yu, Xuetao Guo, Yaping Zhang, Zhuozhi Ouyang, Peng Liu, Chi Zhang, Tiecheng Wang, Hanzhong Jia and Lingyan Zhu, The photodegradation processes and mechanisms of polyvinyl chloride and polyethylene terephthalate microplastic in aquatic environments: important role of clay minerals, Water Research 208 (2022), 117879. https://doi.org/10.1016/j.watres.2021.117879.

[13] A. Ahmed, Y. Chaker, El. H. Belarbi, O. Abbas, J. N. Chotard, H. B. Abassi, A. Nguyen Van Nhien, M. El. Hadri and S. Bresson, XRD and ATR/FTIR investigations of various montmorillonite clays modified by monocationic and dicationic imidazolium ionic liquids, Journal of Molecular Structure 1173 (2018), 653-664. https://doi.org/10.1016/j.molstruc.2018.07.039.

[14] Hongmei Liu, Peng Yuan, Zonghua Qin, Dong Liu, Daoyong Tan, Jianxi Zhu and Hongping He, Thermal degradation of organic matter in the interlayer clay-organic complex: a TG-FTIR study on a montmorillonite/12-aminolauric acid system, Applied Clay Science 80-81 (2013), 398-406. https://doi.org/10.1016/j.clay.2013.07.005.

[15] J. Peyne, J. Gautron, J. Doudeau, E. Joussein and S. Rossignol, Influence of calcium addition on calcined brick clay based geopolymers: a thermal and FTIR spectroscopy study, Construction and Building Materials 152 (2017), 794-803. https://doi.org/10.1016/j.conbuildmat.2017.07.047.

[16] A. Tironi, M. A. Trezza, E. F. Irassar and A. N. Scian, Thermal treatment of kaolin: effect on the pozzolanic activity, Procedia Materials Science 1 (2012), 343-350. DOI: 10.1016/J.MSPRO.2012.06.046.

[17] Morteza Tahmasebi Yamchelou, David Law, Robert Brkljača, Jie Li and Indubhushan Patnaikuni, The effect of pre-treatment and curing temperature on the strength development of alkali-activated clay, Construction and Building Materials 287 (2021), 123000. https://doi.org/10.1016/j.conbuildmat.2021.123000.

[18] E. Görlich, The structure of SiO_2 - current views, Ceramics International 8(1) (1982), 3-16. https://doi.org/10.1016/0272-8842(82)90009-8.

[19] J. T. Kloprogge, Application of vibrational spectroscopy in clay minerals synthesis, Developments in Clay Science 8 (2017), 222-287. https://doi.org/10.1016/B978-0-08-100355-8.00008-4.

[20] Zhen Wang, Shifeng Dai, Jianhua Zou, David French and Ian T. Graham, Rare earth elements and yttrium in coal ash from the Luzhou power plant in Sichuan, Southwest China: concentration, characterization and optimized extraction, International Journal of Coal Geology 203 (2019), 1-14. https://doi.org/10.1016/j.coal.2019.01.001.